

Original Research

Development of Nonlinear FEA Method for 3D-Printed Polymeric Porous Structures

Xiangxiang Meng¹ , Mitsugu Todo^{2,*} 

¹ Interdisciplinary Graduate School of Engineering Sciences, Kyushu University 6-1 Kasuga-koen, Kasuga, Fukuoka 816-8580, Japan; meng.xiangxiang.901@s.kyushu-u.ac.jp

² Research Institute for Applied Mechanics, Kyushu University 6-1 Kasuga-koen, Kasuga, Fukuoka 816-8580, Japan

* Correspondence: todo@riam.kyushu-u.ac.jp

Received: 10 September 2025 / Accepted: 20 December 2025 / Published online: 7 January 2026

Abstract

Three-dimensional printing technology has been widely utilized to construct a variety of complex biomimetic structures. A target structure is designed using 3D-CAD and then the CAD data are sent to the control unit of a 3D-printed machine to fabricate a corresponding real structure. Recently, finite element analysis (FEA) installed into 3D-CAD can be used to assess the structural integrity of the designed structures. However, it is still difficult to analyze the nonlinear mechanical responses using FEA. The aim of the present study is to develop a nonlinear FEA method to characterize the elastic-plastic deformation behaviors along with micro-damage formation in 3D-printed polymeric porous structures. It was found that the proposed FEA method can reasonably be used to predict the nonlinear behaviors of two different types of 3D-printed porous structures under compressive loading. Mechanical properties such as stiffness, fracture energy and strength were also well predicted by FEA. The micro-fracture processes of the real structures were well characterized by the damage models with FEA including the tensile cracking with the maximum principal stress criterion and the compressive crushing with the minimum principal strain criterion. These results demonstrated the effectiveness and originality of the developed nonlinear FEA framework in predicting the deformation and damage behavior of polymeric porous structures.

Keywords: 3D-printing, finite element analysis, porous polymer structure, nonlinear mechanical response, micro-damage formation

1. Introduction

Three-dimensional printing technology has been widely utilized to construct a variety of complex structures imitating unique structures existing in nature in the field of biomimetic engineering (Li et al., 2024; Siddique et al., 2022; Wang et al., 2020; Yan et al., 2021). Different types of engineering materials such as metals (Attarilar et al., 2021; Vafadar et al., 2021), ceramics (Chen et al., 2024; Kostretsova et al., 2024) and polymers (Fang et al., 2023; Ma et al., 2024) can be used as the source materials in 3D-printed technology. In the standard constructing method, a target structure is designed using Three-dimensional computer-aided design (3D-CAD) software and then the prepared CAD data is sent to the control unit of a 3D-printed machine to fabricate a corresponding real structure. Then, to assess its durability and safety under the expected environmental conditions, physical and chemical properties of the constructed structure must be examined through different kinds of experimental methods before it is provided for actual use. Among the physical properties, the mechanical properties related to deformation and fracture behaviors are of the most fundamental and important properties that must be carefully examined in order to understand its structural safety. If one finds some problems, then the design concept will be modified so that the structural integrity is improved.

On the other hand, finite element analysis (FEA) has been widely used in the design process of engineering structures to assess their structural integrity (Cipriani et al., 2021; Naghavi et al., 2022; Saleh et al., 2022; Santiago et al., 2023). Some well-known FEA codes are available for nonlinear and dynamic analyses, while basic FEA codes have been directly installed into most commercial 3D-CAD



software so that the mechanical assessment of the designed structure can be conducted using the same software. In the current FEA technology, it may be concluded that the method of linear elastic analysis has been perfectly established with the limitation of small scale deformation. Therefore, the linear elastic behaviors of 3D-printed structures can clearly be understood by using the 3D-CAD/FEA system under the designing stage. However, methods for nonlinear analyses targeting approximated solutions of nonlinear problems such as plastic deformation and micro-damage formation with high accuracy have not been well established yet. It is thus very difficult to characterize the nonlinear deformation behaviors of 3D-printed structures by the nonlinear FEA. If such nonlinear FEA method is established, it will be one of the most useful tools in the 3D-printed technology.

The primary aim of the present study is to develop nonlinear FEA method to characterize the elastic-plastic deformation behaviors along with micro-damage formations of 3D-printed polymeric porous structures. Two different types of porous structure were designed using 3D-CAD software and then constructed using a 3D-printer with an acrylic resin. Their compressive deformation and fracture behaviors were then characterized through compression tests. In the meantime, nonlinear finite element analyses of the porous structures were also performed using a commercial FEA software and the corresponding CAD data. The analytical results were compared with the experimental results in order to assess the accuracy of the proposed nonlinear method.

2. Experimental methods

2.1. Specimen preparation

Two different simple porous structures were designed using AutoCAD software as shown in Fig. 1. The design of these structures was inspired by the Bouligand structure found in the exoskeleton of mantis shrimp. The model was simplified to retain the fundamental features of the natural structure, namely the stacked and rotated tubular arrangement. In addition, two different sizes were designed to verify the influence of size on the accuracy of the experimental results. Then, the CAD data were sent to the control unit of a 3D printer (ProJet®3500 HD Max, 3D Systems) and specimens for compression testing were fabricated with an acrylic resin (VisiJet® M3C Crystal, 3D Systems). The printer has a spatial resolution of $375 \times 375 \times 790$ dpi ($X \times Y \times Z$) and a layer thickness of $32 \mu\text{m}$ in the HD mode, enabling precise fabrication of fine structural features. Stereolithography has been introduced in this commercial 3D-printer, in which the acrylic monomer is cured under ultraviolet light. Wax is also used as structural support and removed after 3D-printed by heating the specimens at 60°C . The fabricated specimens are shown in Fig. 2. At least three specimens were prepared for the compression tests. The two kinds of specimens are called Model 1 and Model 2, hereafter.

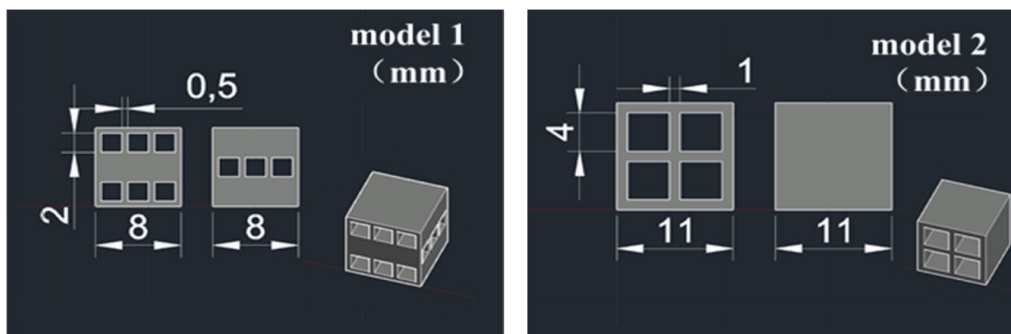


Fig. 1. Original designs of two simple porous models.



Fig. 2. 3D-printed porous structures; right: Model 1 and left: Model 2.

2.2. Compression test

Compression tests of the specimens were conducted using a conventional testing machine (EZ-Test, Shimadzu Co., Kyoto, Japan) at a constant speed of 6 mm/min. The testing setup is shown in Fig. 3. Load-time and displacement-time data were then recorded in the control unit with a personal computer. Load-displacement relations were obtained from the recorded data. The stiffness of a specimen was evaluated as the slope of the initial straight portion of the corresponding load-displacement curve. Compressive strength and fracture energy were also evaluated by measuring the maximum load and the area under the load-displacement curve up to the complete fracture point.

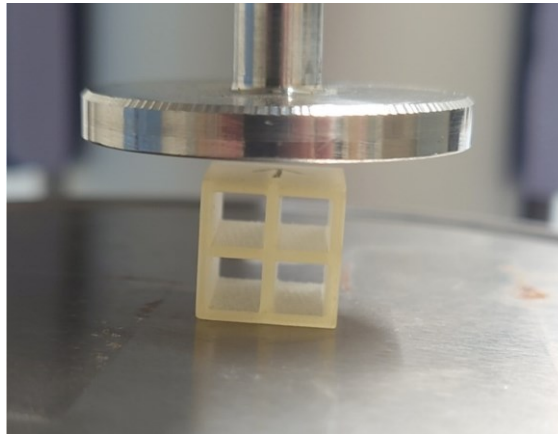


Fig. 3. Set up of compression testing.

2.3. Fracture characterization

The damaged regions of the tested specimens were observed using a field emission scanning electron microscope (FE-SEM S-4200, Hitachi, Ltd., Japan) in order to characterize the deformation and fracture mechanisms. The specimens were mounted on aluminium stages and sputter-coated with Pt-Pd using an ion sputter coater (E-1030, Hitachi, Ltd., Japan) prior to SEM observation.

3. Finite element analysis

3.1. Basic theory of deformable material

A mechanical model of a deformable body was introduced into FEA in this study, and the corresponding schematic stress-strain responses up to the fracture points are shown in Fig. 4 under simple uniaxial tensile and compressive stress conditions. The tensile stress-strain response was assumed to be linear elastic without plastic deformation. It was also assumed that the tensile fracture, called ‘tensile cracking’, takes place when the maximum principal stress reaches its critical value.

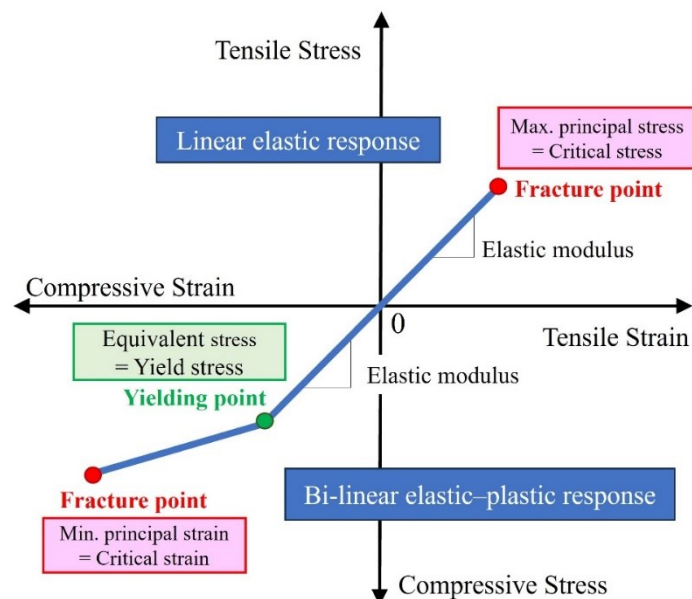


Fig. 4. Mechanical model used for the 3D-printed structures.

On the contrary, the compressive stress-strain response of the resin was assumed to be characterized by an elastic-plastic model. The linear elastic theory was used for the elastic part, while the plastic part was also approximated by a linear response with the reduced slope, called the strain hardening coefficient, of the stress-strain response. The von Mises equivalent stress was utilized to assess the onset of yielding under compressive stress states, while the compressive fracture, called ‘compressive crushing’, was assumed to take place when the minimum principal strain reaches its critical value. This mechanical theory has been implemented into a commercial FEA code, Mechanical Finder (RCCM Co., Ltd., Japan).

3.2. Finite element modeling

The CAD data of the two models were used to construct finite element models in Mechanical Finder. Mesh generation of the models was automatically conducted using 4-node tetrahedral elements. To determine an appropriate mesh size, several mesh divisions of 0.8 mm, 0.7 mm, 0.5 mm, 0.4 mm, and 0.3 mm were tested for Model 1. The corresponding maximum loads obtained from the simulations were 503 N, 439 N, 410 N and 403 N, respectively. When the minimum element size was set to 0.3 mm, the finite element analysis failed to converge. Therefore, the minimum element size was set to 0.5 mm in this study. The numbers of elements and nodes were 24,795 and 6,872 for Model 1, and 66,658 and 14,163 for Model 2, respectively. To replicate the actual compression testing procedure, metal plate models were positioned both above and below the specimen models so that the specimens were sandwiched between two metallic plates, as shown in Fig. 5.

The mechanical theory described above has been implemented into the FEA code. It should be noted that in general, realistic fracture behavior such as cracking cannot be expressed in FEA. In this analysis, if in an element, the average maximum principal stress or the average minimum principal strain reaches its critical value under a tensile or compressive stress condition, then the element was recognized as a fracture element and the stiffness of the element was reduced to the very small value close to zero so that the element could not support tensile stress or compressive stress anymore. The material properties such as elastic modulus, Poisson’s ratio, critical stress at tensile fracture, compressive yield stress, work hardening coefficient and critical strain at compressive fracture are shown in Table 1.

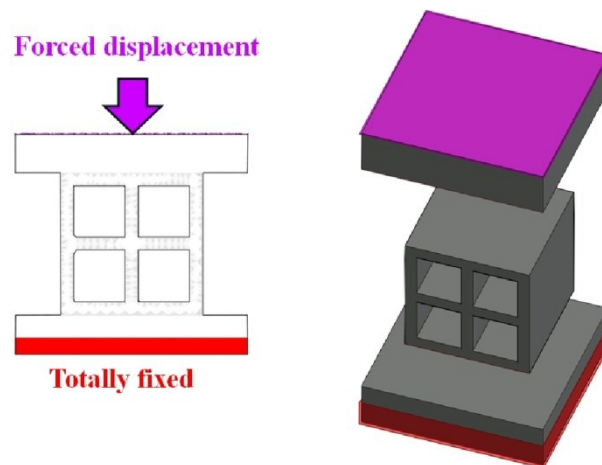


Fig. 5. Boundary conditions used in FEA.

Table 1. Material constants used in FEA.

Material	Elastic modulus	Poisson’s ratio	Critical tensile stress	Compressive yield stress	Work hardening coefficient	Critical compressive strain
Model 1	580 MPa	0.39	30 MPa	60 MPa	0.29	0.12
Model 2	580 MPa	0.39	30 MPa	60 MPa	0.29	0.2
Plate	196 GPa	0.34	-	-	-	-

4. Results and discussion

4.1. Compression testing results

Load-displacement curves obtained from the compression tests are shown in Fig. 6. For each model, testing results of three specimens are shown in the graphs. It can be said that the reproducibility was reasonably good for both models. In Model 1, the load decreased rapidly just after it reached the peak value, suggesting a brittle fracture behavior. On the contrary, in Model 2, the load gradually decreased

after it reached the peak value, indicating better durability than model 1. The stiffness, the fracture energy, and the strength were evaluated from the load-displacement relations and are shown in Table 2.

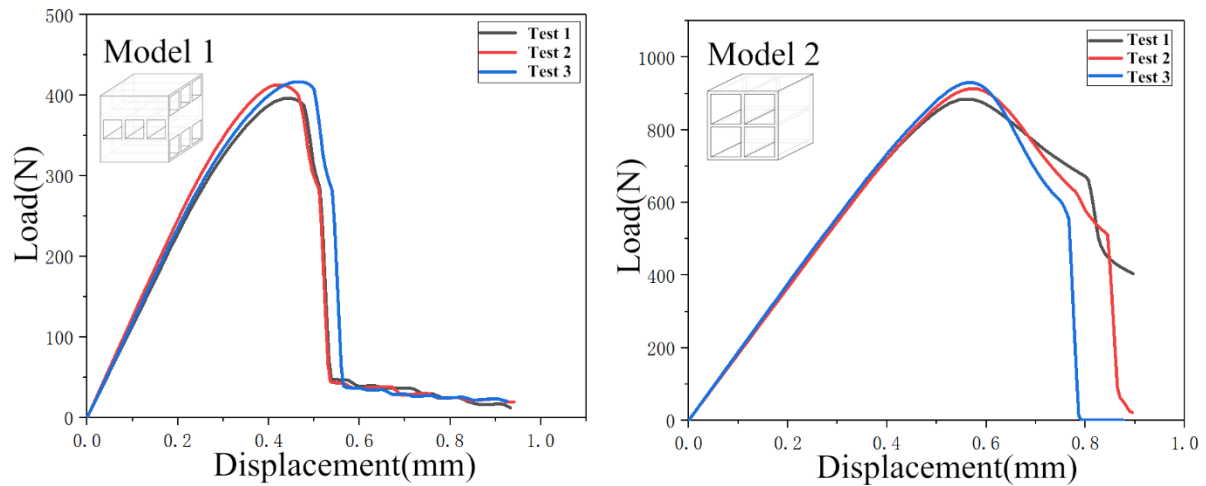


Fig. 6. Load-displacement curves under compressive loading condition.

Table 2. Mechanical properties obtained from compression tests and FEA.

Model	Source	Stiffness, N/mm	Fracture energy, J	Strength, N
Model 1	Experimental	1160 ± 52.9	0.139 ± 0.008	406.7 ± 14.3
	FEA	1061	0.129	410.1
Model 2	Experimental	1844 ± 15.5	0.290 ± 0.006	909.4 ± 23.0
	FEA	1899	0.354	865.5

4.2. Fracture behavior and mechanism

Overviews of specimens at fracture are shown in Fig. 7. Both models exhibited brittle fracture behavior. It was confirmed that the fractures mainly took place in the corners of the porous structures. It was expected that stress concentrations were easily generated at those corners, resulting in the localized fractures.

SEM micrographs of the fracture regions are shown in Fig. 8. Brittle microcracks were initiated at the localized stress concentration points and propagated without generation of plastic deformation in both models.

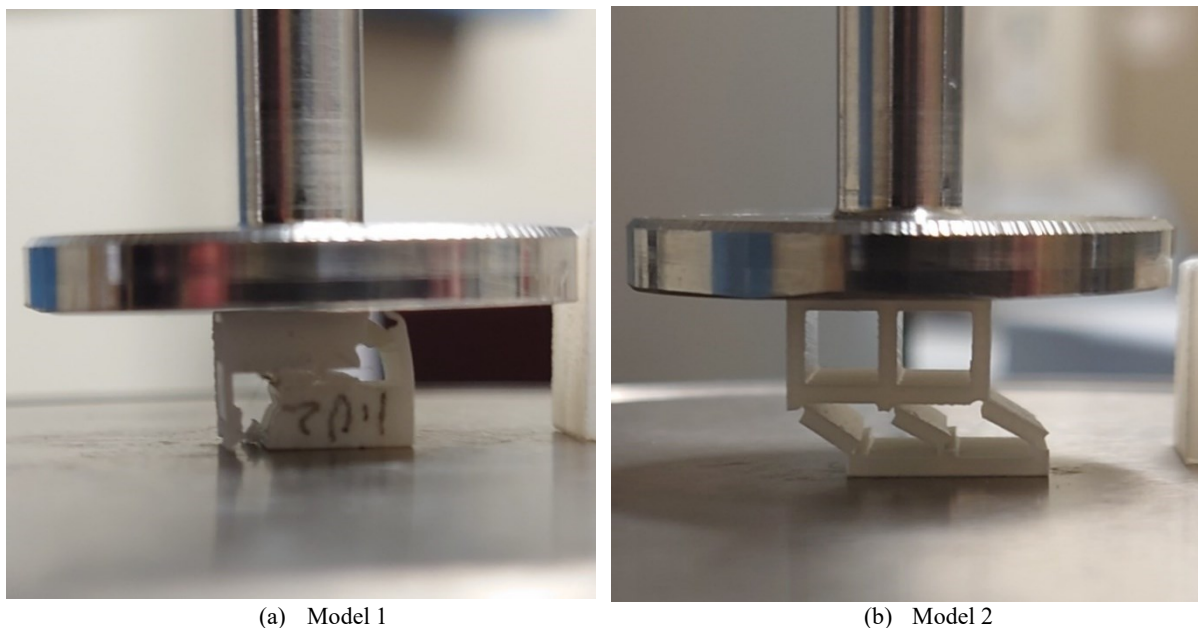


Fig. 7. Compressive fracture behaviors of the testing specimens.

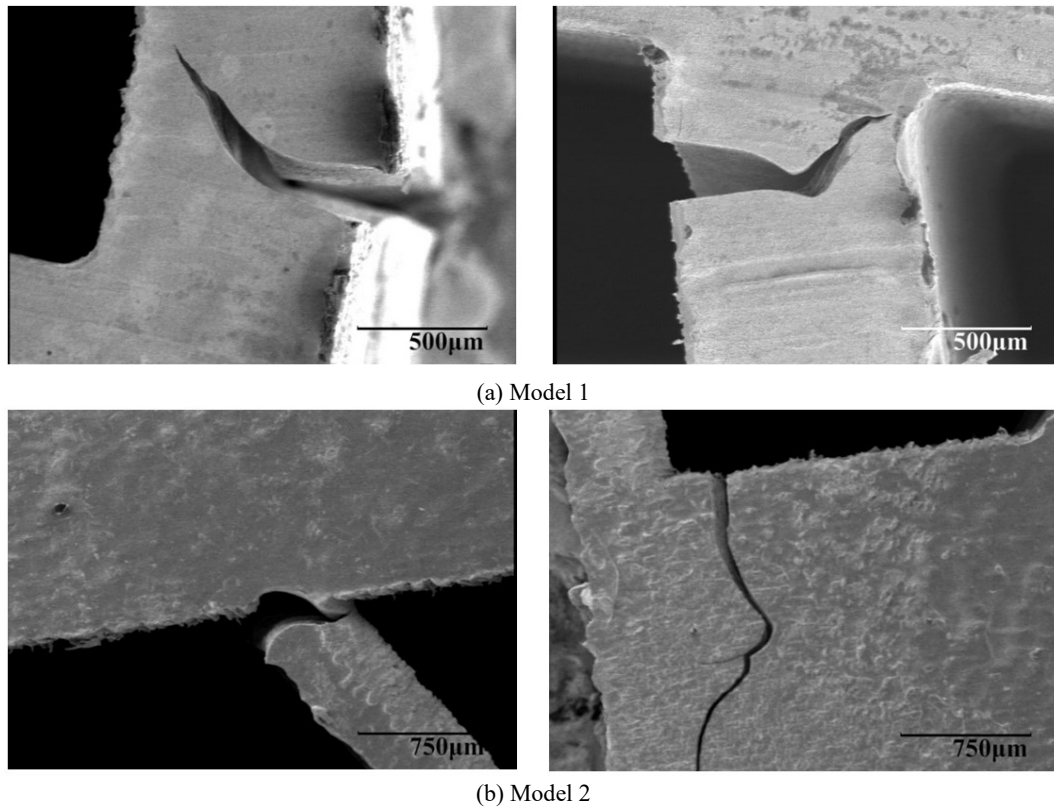


Fig. 8. SEM micrographs of fracture behaviors.

4.3. FEA results of load-displacement curves

Load-displacement curves obtained from FEA are shown along with the typical experimental results in Fig. 9. In model 1, the FEA result coincided with the typical experimental result very well. The stiffness and the strength (maximum load) were almost identical to the experimental, and especially the rapid reduction of load at the fracture point was well reproduced in FEA. This result suggested that the damage model used in FEA can reasonably reproduce the fracture behavior of the real specimen. On the contrary, in Model 2, although the stiffness and the maximum load well coincided with the experimental; however, the reduction behavior of load after the peak point was different. The sudden reduction of load in FEA suggested that the theoretical damage modeling could not well express the slow accumulation of damage in the actual Model 2 specimen.

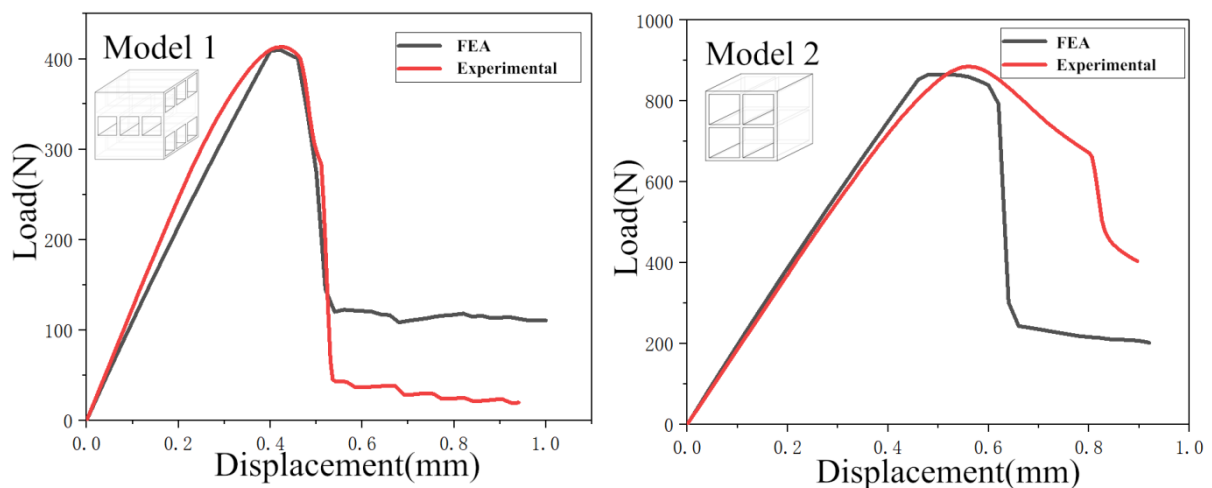


Fig. 9. Comparison of load-displacement curves for a) Model 1 and b) Model 2.

4.4. Distribution of fracture elements and mechanical properties

The numbers of elements subjected to tensile cracking, compressive yielding and compressive crushing are shown in Table 3. It is clearly seen that in Model 2, the tensile cracking was most dominant of the three damage modes. This result was well coincided with the microcrack generation as shown in

Fig. 8. On the other hand, in Model 1, compressive crushing was also observed and the number of the crashed elements was very close to that of the cracking elements.

Table 3. The numbers of elements suffered by tensile cracking, compressive yielding, and compressive crushing.

Model	Tensile cracking	Compressive yielding	Compressive crushing
Model 1	563	76	491
Model 2	6618	606	249

Distribution patterns of elemental fractures and the corresponding mechanical parameters in Model 1 are shown in Fig. 10. For Model 1, tensile failure is primarily concentrated in the transverse members of the middle layer, which corresponds well to the regions of high maximum principal stress. This behaviour arises from the angular arrangement between the middle and adjacent layers, which interrupts the vertical load path. Consequently, the redirected stress flow induces a combination of bending stress and local tensile stress in the middle layer, leading to tensile cracking in these regions. In contrast, the minimum principal strain is concentrated near the junctions between the vertical and transverse members of the middle layer. These regions sustain significant compressive loads along the vertical direction and therefore undergo compressive crushing. A similar trend is observed in the experimental results shown in Fig. 7, where the middle layer of Model 1 exhibited severe damage: the vertical segments fractured at their joints, and the transverse parts failed on both sides. This experimental observation is in good agreement with the finite element analysis results.

Distribution patterns of elemental fractures and the corresponding mechanical parameters in Model 2 are shown in Fig. 11. Both the tensile cracking and the compressive crushing were mainly concentrated at the inner corners, where the max. principal stress and the min. principal strain also showed high concentrations. It might be considered that in Model 2, the tensile cracking were rapidly accumulated at the corners, resulting in the fast loss of structural integrity and therefore the sudden reduction of load after the peak load point as shown in Fig. 9. In the actual 3D-printed Model 2, the damage accumulation at the corners progressed more slowly, resulting the slow reduction of load after the peak load point as shown in Fig. 6.

The three mechanical properties such as the stiffness, the fracture energy and the strength were evaluated from the FEA results and are shown in Table 2 along with the experimental results. It is clearly seen that the agreements between the FEA and the experimental were pretty good, suggesting the high accuracy of FEA with the proposed mechanical model described in the section 3.1.

5. Conclusions

Two different types of simple polymeric porous structures were designed using 3D-CAD and fabricated using 3D-printer with an acrylic resin. Their mechanical properties were then characterized under compressive loading condition. FEA of the two models was also conducted with use of the nonlinear mechanical theory of deformable body. The experimental and analytical results were then compared to validate the applicability of the current nonlinear FEA model. The conclusions were obtained as follows:

- 1) The experimental compressive load-displacement curves of the two models were well reproduced by the FEA models. Especially, in Model 1, the rapid reduction of load just after the peak load point can nicely be imitated by introducing the fracture models under tensile and compressive stress conditions.
- 2) The main fracture mechanisms were found to be localized tensile cracking and compressive crushing in Model 1, while the tensile cracking at the inner corners was most dominant in Model 2. The tensile cracking were also clearly observed by SEM in both 3D-printed models.
- 3) For both Model 1 and Model 2, the compressive mechanical properties such as the stiffness, the fracture energy and the compressive strength were well predicted by the FEA models.
- 4) It was clearly confirmed the the proposed FEA model with the nonlinear mechanical model can be very useful to analyze the compressive mechanical behavior of 3D-printed porous structures.

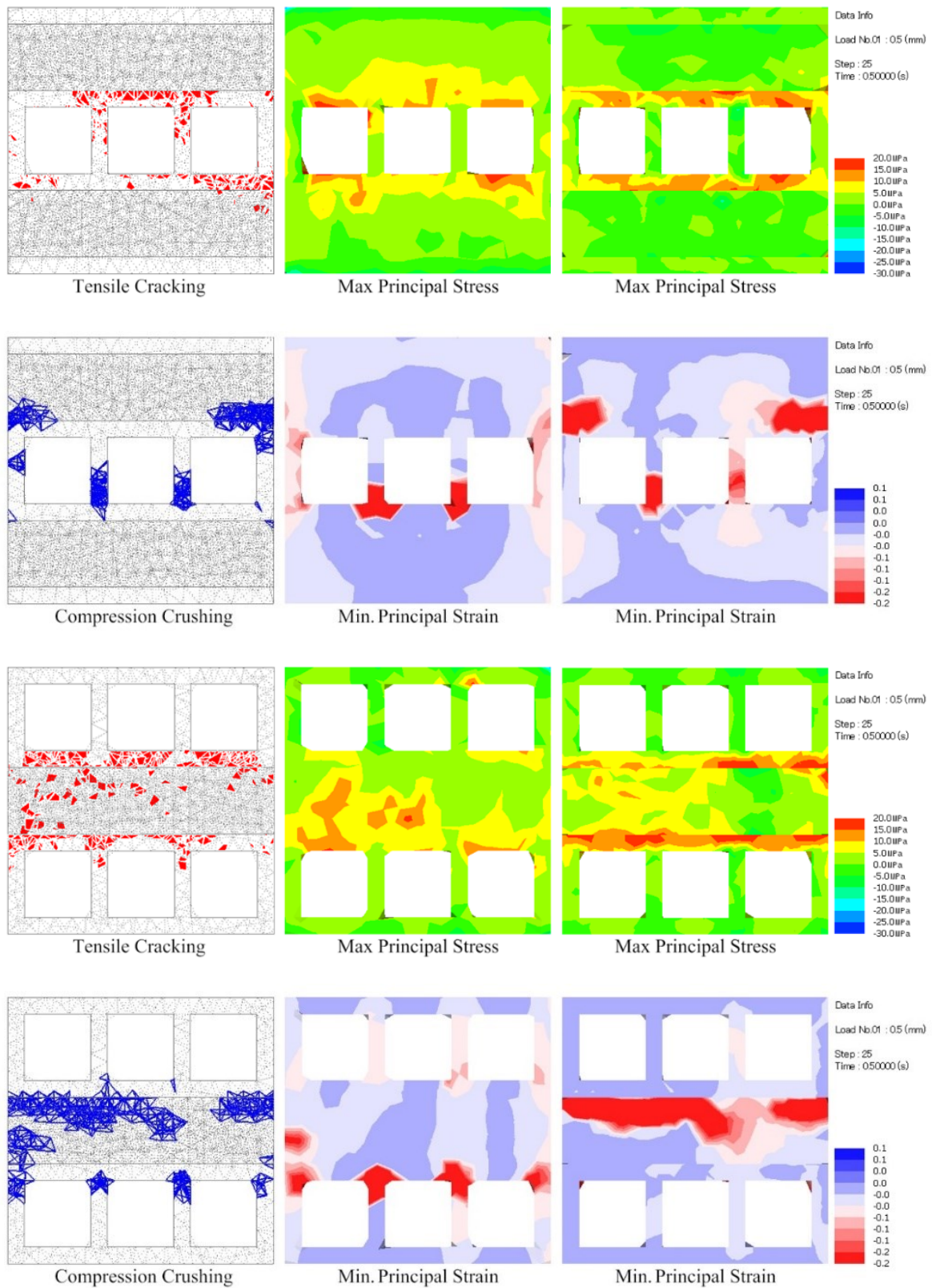


Fig. 10. Distribution patterns of elemental fractures and corresponding mechanical parameters in Model 1.

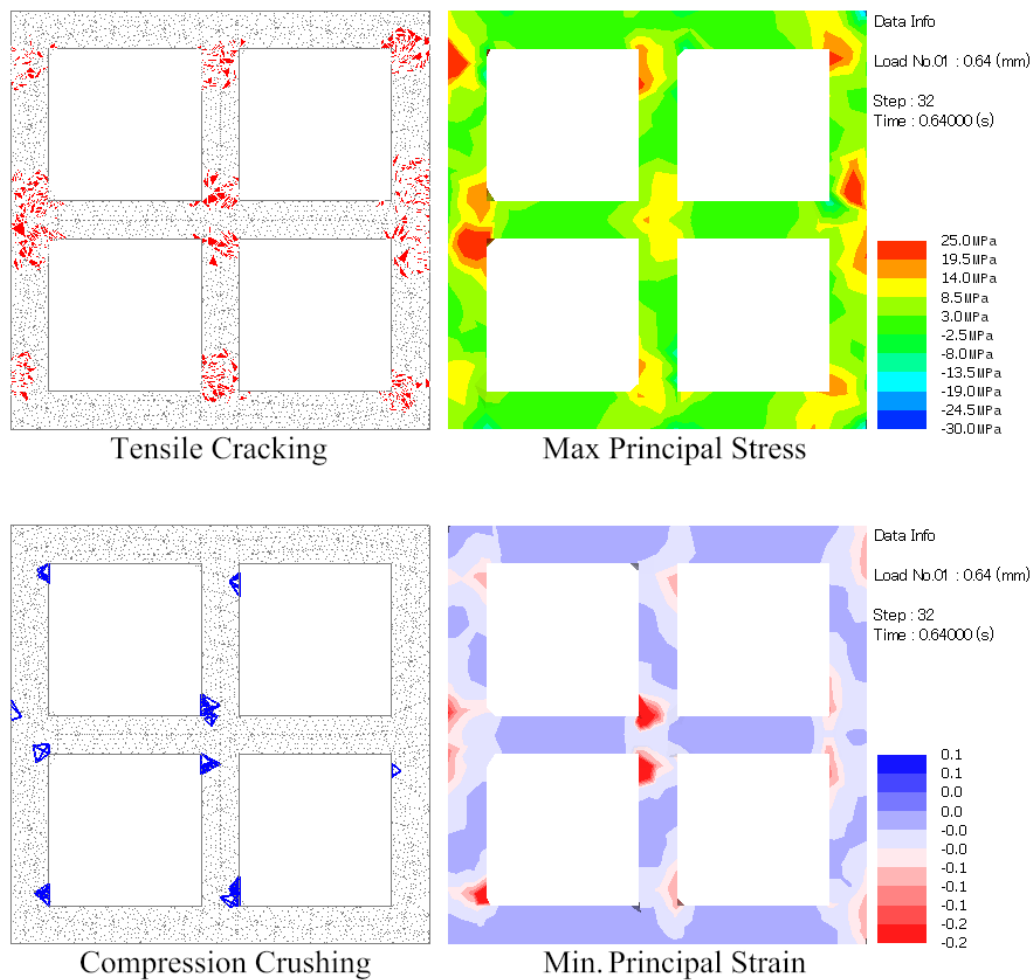


Fig. 11. Distribution patterns of elemental fractures and corresponding mechanical parameters in Model 2.

Declarations

Authors' contributions: Mitsugu Todo contributed to the conceptualization and methodology; Xiangxiang Meng contributed to the experiments, finite element analysis and original draft preparation. All authors have proofread and edited the whole manuscript. All authors have read and agreed to the published version of the manuscript.

Funding: This research received no external funding.

Declaration of competing interest: The authors declare that they have no known competing financial interests or personal relationships that could have appeared to influence the work reported in this paper.

Data availability statement: The data that support the findings of this study are available from the corresponding author upon reasonable request.

References

- Attarilar, S., Ebrahimi, M., Djavanroodi, F., Fu, Y., Wang, L., & Yang, J. (2021). 3D printing technologies in metallic implants: A thematic review on the techniques and procedures. *International Journal of Bioprinting*, 7(1), Article 306. <https://doi.org/10.18063/ijb.v7i1.306>
- Chen, Y., Quan, S., Huang, S., Liu, W., Chen, Z., Liu, J., Li, C., & Yang, H. (2024). Applications and progress of 3D-printed bioceramic scaffolds in bone tissue repair and immune regulation. *Ceramics International*, 50(23), 48891–48908. <https://doi.org/10.1016/j.ceramint.2024.09.294>
- Cipriani, C. E., Ha, T., Martinez Defilló, O. B., Myneni, M., Wang, Y., Benjamin, C. C., Wang, J., Pentzer, E. B., & Wei, P. (2021). Structure–processing–property relationships of 3D printed porous polymeric materials. *ACS Materials Au*, 1(1), 69–80. <https://doi.org/10.1021/acsmaterialsau.1c00017>

- Fang, W., Yang, M., Wang, L., Li, W., Liu, M., Jin, Y., Wang, Y., Yang, R., Wang, Y., Zhang, K., & Fu, Q. (2023). Hydrogels for 3D bioprinting in tissue engineering and regenerative medicine: Current progress and challenges. *International Journal of Bioprinting*, 9(5), Article 759. <https://doi.org/10.18063/ijb.759>
- Kostretsova, N., Pesce, A., Anelli, S., Nuñez, M., Morata, A., Smeacetto, F., Torrella, M., & Tarancón, A. (2024). Single-step fully 3D printed and co-sintered solid oxide fuel cells. *Journal of Materials Chemistry A*, 12(34), 22960-22970. <https://doi.org/10.1039/D4TA02490G>
- Li, J., Li, M., Koh, J. J., Wang, J., & Lyu, Z. (2024). 3D-printed biomimetic structures for energy and environmental applications. *DeCarbon*, 3, Article 100026. <https://doi.org/10.1016/j.decarb.2023.100026>
- Ma, T., Zhang, Y., Ruan, K., Guo, H., He, M., Shi, X., Guo, Y., Kong, J., & Gu, J. (2024). Advances in 3D printing for polymer composites: A review. *InfoMat*, 6(6), Article e12568. <https://doi.org/10.1002/inf2.12568>
- Naghavi, S. A., Tamaddon, M., Marghoub, A., Wang, K., Babamiri, B. B., Hazeli, K., Xu, W., Lu, X., Sun, C., Wang, L., Moazen, M., Wang, L., Li, D., & Liu, C. (2022). Mechanical characterisation and numerical modelling of TPMS-based gyroid and diamond Ti6Al4V scaffolds for bone implants: An integrated approach for translational consideration. *Bioengineering*, 9(10), Article 504. <https://doi.org/10.3390/bioengineering9100504>
- Saleh, M., Anwar, S., Al-Ahmari, A. M., & Alfaify, A. (2022). Compression performance and failure analysis of 3D-printed carbon fiber/PLA composite TPMS lattice structures. *Polymers*, 14(21), Article 4595. <https://doi.org/10.3390/polym14214595>
- Santiago, R., Ramos, H., AlMahri, S., Banabila, O., Alabdouli, H., Lee, D. W., Aziz, A., Rajput, N., Alves, M., & Guan, Z. (2023). Modelling and optimisation of TPMS-based lattices subjected to high strain-rate impact loadings. *International Journal of Impact Engineering*, 177, Article 104592. <https://doi.org/10.1016/j.ijimpeng.2023.104592>
- Siddique, S. H., Hazell, P. J., Wang, H., Escobedo, J. P., & Ameri, A. A. H. (2022). Lessons from nature: 3D printed bio-inspired porous structures for impact energy absorption – A review. *Additive Manufacturing*, 58, Article 103051. <https://doi.org/10.1016/j.addma.2022.103051>
- Vafadar, A., Guzzomi, F., Rassau, A., & Hayward, K. (2021). Advances in metal additive manufacturing: A review of common processes, industrial applications, and current challenges. *Applied Sciences*, 11(3), Article 1213. <https://doi.org/10.3390/app11031213>
- Wang, D., Chen, D., & Chen, Z. (2020). Recent progress in 3D printing of bioinspired structures. *Frontiers in Materials*, 7, Article 286. <https://doi.org/10.3389/fmats.2020.00286>
- Yan, X., Bethers, B., Chen, H., Xiao, S., Lin, S., Tran, B., Jiang, L., & Yang, Y. (2021). Recent advancements in biomimetic 3D printing materials with enhanced mechanical properties. *Frontiers in Materials*, 8, Article 518886. <https://doi.org/10.3389/fmats.2021.518886>

Rozwój Nieliniowej Metody MES dla Porowatych Struktur Polimerowych Drukowanych w Technologii 3D

Streszczenie

Technologia druku trójwymiarowego jest szeroko wykorzystywana do konstruowania różnorodnych złożonych struktur biomimetycznych. Struktura docelowa jest projektowana za pomocą 3D-CAD, a następnie dane CAD są przesyłane do jednostki sterującej maszyny drukującej w 3D w celu wytworzenia odpowiadającej im rzeczywistej struktury. Od niedawna, metoda elementów skończonych (MES) dostępna w programach 3D-CAD, może być używana do oceny integralności strukturalnej projektowanych struktur. Analiza nieliniowych odpowiedzi mechanicznych za pomocą MES jest utrudniona. Celem niniejszego badania jest opracowanie nieliniowej metody MES do scharakteryzowania zachowań odkształceń sprężysto-plastycznych wraz z powstawaniem mikrouszkodzeń porowatych struktur polimerowych drukowanych w technologii 3D. Stwierdzono, że proponowana metoda MES może być w uzasadniony sposób wykorzystana do przewidywania nieliniowych zachowań pod obciążeniem ściskającym dwóch różnych typów porowatych struktur drukowanych w technologii 3D. Właściwości mechaniczne, takie jak sztywność, energia pęknięcia i wytrzymałość, zostały również wyznaczone za pomocą MES. Procesy mikropęknięć rzeczywistych struktur zostały odpowiednio scharakteryzowane za pomocą modeli uszkodzeń z wykorzystaniem MES, obejmujących pęknięcie przy rozciąganiu z kryterium maksymalnego naprężenia głównego oraz pęknięcie przy ściskaniu z kryterium minimalnego odkształcenia głównego. Wyniki te dowiodły skuteczności i oryginalności opracowanego nieliniowego modelu MES w przewidywaniu odkształceń i uszkodzeń porowatych struktur polimerowych.

Słowa kluczowe: drukowanie 3D, analiza elementów skończonych, porowata struktura polimerowa, nieliniowa odpowiedź mechaniczna, powstawanie mikrouszkodzeń
